

UCRL-JC-125360

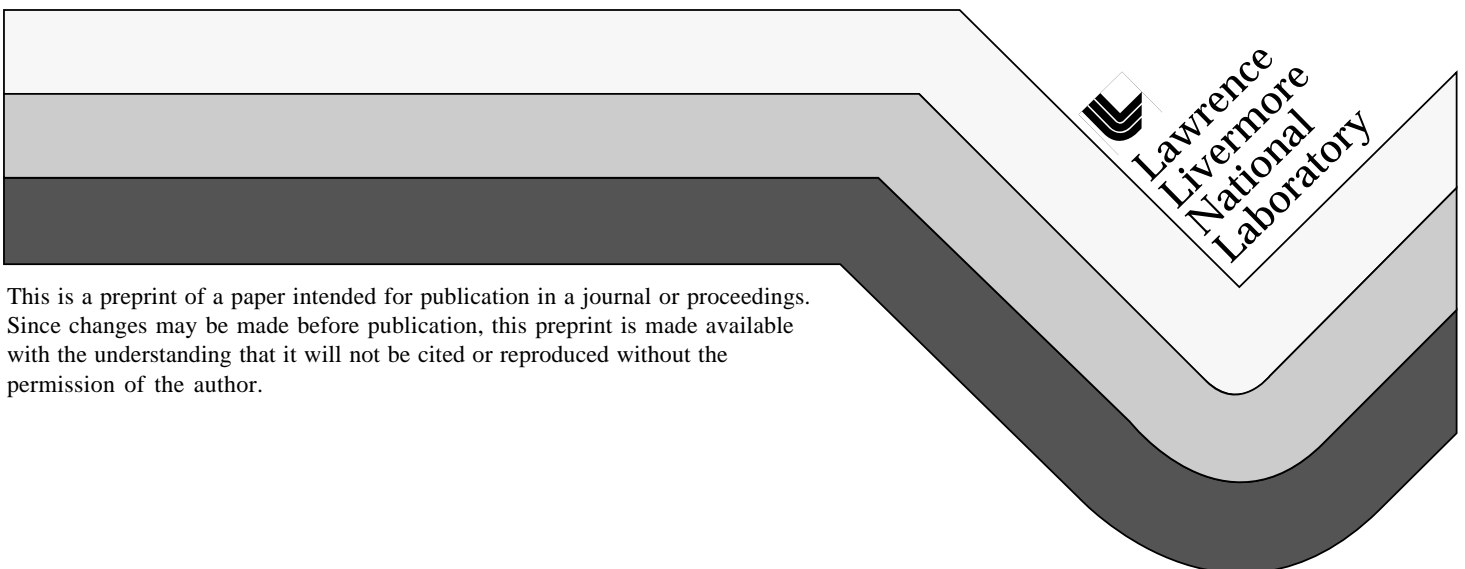
PREPRINT

High-Resolution X-Ray Spectra from Low-Temperature, Highly Charged Ions

P. Beiersdorfer

This paper was prepared for submittal to the
Proceedings of the 17th International Conference
on X-Ray and Innershell Processes
Hamburg, Germany
September 9-13, 1996

September 3, 1996



DISCLAIMER

This document was prepared as an account of work sponsored by an agency of the United States Government. Neither the United States Government nor the University of California nor any of their employees, makes any warranty, express or implied, or assumes any legal liability or responsibility for the accuracy, completeness, or usefulness of any information, apparatus, product, or process disclosed, or represents that its use would not infringe privately owned rights. Reference herein to any specific commercial product, process, or service by trade name, trademark, manufacturer, or otherwise, does not necessarily constitute or imply its endorsement, recommendation, or favoring by the United States Government or the University of California. The views and opinions of authors expressed herein do not necessarily state or reflect those of the United States Government or the University of California, and shall not be used for advertising or product endorsement purposes.

High-Resolution X-Ray Spectra from Low-Temperature, Highly Charged Ions

Peter Beiersdorfer

*Department of Physics and Space Technology
Lawrence Livermore National Laboratory, Livermore, CA 94550, USA*

Abstract. The electron beam ion traps (EBIT) at Livermore were designed for studying the x-ray emission of highly charged ions produced and excited by a monoenergetic electron beam. The precision with which the x-ray emission can be analyzed has recently been increased markedly when it became possible to decouple the temperature of the ions from the energy of the electron beam by several orders of magnitude. By adjusting the trap parameters, ion temperatures as low as 15.8 ± 4.4 eV for Ti^{20+} and 59.4 ± 9.9 eV for Cs^{45+} were achieved. These temperatures were more than two orders of magnitude lower than the energy of the multi-keV electron beam used for the production and excitation of the ions. A discussion of the techniques used to produce and study low-temperature highly charged ions is presented in this progress report. The low ion temperatures enabled measurements heretofore impossible. As an example, a direct observation of the natural line width of fast electric dipole allowed x-ray transitions is described. From the observed natural line width and by making use of the time-energy relations of the uncertainty principle we were able to determine a radiative transition rate of 1.65 fs for the $2p$ - $3d$ resonance transition in neonlike Cs^{45+} . A brief discussion of other high-precision measurements enabled by our new technique is also given.

INTRODUCTION

A reduction in the velocity of an atom increases the spectroscopic precision and creates the opportunity for new classes of observations. This has now been shown extensively in the case of trapped atoms, molecules, and singly charged ions cooled by lasers [1,2]. Undoubtedly, the spectroscopy of *highly* charged ions can benefit from a reduction of the ion motion as well. The increase in the spectroscopic precision associated with the preparation of cool, highly charged ions enables measurements of the energy levels with greater accuracy for precise determinations of quantum electrodynamical effects, of

nuclear parameters, or of line coincidences for photopumping of x-ray lasers. It enables the study of line shapes and the application of laser spectroscopy.

We report on experiments performed on the electron beam ion trap (EBIT) facilities at the Lawrence Livermore National Laboratory that have systematically lowered the thermal motion of trapped, highly charged ions [3,4]. The reduction in thermal motion is carried out to the point where the observed x-ray line width of fast electric dipole transitions is limited by the Heisenberg uncertainty relations and the Lorentzian line shape is observed. In these experiments, a decoupling on the order of 100 times is achieved between the kinetic energy of the ions and the energy of the electron beam used for excitation of the observed x-ray lines. Such a marked decoupling is needed because the natural line width is a much smaller fraction of the transition energy for x-ray lines than for lines in the ultraviolet or visible, given the same lifetimes of the relevant levels. Observations of the Lorentzian line shape of x-ray lines from highly charged ions further enlarge the arsenal of precision spectroscopic observations available to atomic physicists, complementing, for example, such observations in neutral or few-times ionized ions excited by synchrotron sources [5].

Measuring the width of the Lorentzian line shape allows us to determine the radiative transition rates of fast, electric dipole allowed resonance transitions. Existing techniques for measuring fast transition rates fail to yield results for lifetimes shorter than a few picoseconds [6,7]. With our technique we measure lifetimes in the femtosecond range, i.e., in a regime that is 1000 times faster and has never before been open to experimental scrutiny. Resonance transitions with a radiative lifetime shorter than 10 femtoseconds are found, for example, among the K-shell transitions of heliumlike ions above argon ($Z=18$) and among the L-shell transitions of neonlike ions above krypton ($Z=36$). In other words, femtosecond radiative lifetimes are common for most resonance transitions in highly charged ions. These transitions form the dominant lines in a given x-ray spectrum and play an important role in the density and temperature diagnostics of high-temperature plasmas, such as those found in laser-produced, tokamak, and astrophysical plasmas [8–11]. Because fast transition rates correspond to large absorption oscillator strengths, these resonance transitions dominate the Planck mean opacity of a high-temperatures plasma, and accurate knowledge of their radiative rates is important for plasma opacity and line transfer [12,13]. Measurements of the radiative lifetimes of these fast resonance transitions are needed to validate atomic physics calculations. Unlike transition energy measurements, they test the long-range behaviour of atomic wave functions and thus complement atomic structure measurements.

The electron beam ion trap devices are well suited for the spectroscopy of isolated spectral lines from highly charged ions. Because the devices employ a quasi monoenergetic electron beam for the production and excitation of highly charged ions, the charge state of interest and the excitation process can be selected by the appropriate choice of the electron beam energy [14].

Line blending can thus be avoided. Most importantly, line broadening caused by dielectronic satellite transitions with high- n spectator electrons, which is a common occurrence in most high-temperature plasma sources [15,16], can be avoided easily. Density and opacity broadening, which may broaden x-ray lines, for example, in laser-produced plasmas [17], are also not an issue because of the relatively low density of the electron beam ($\leq 5 \times 10^{12} \text{ cm}^{-3}$). Directional ion motion, as found in heavy-ion accelerators, does not occur in electron beam ion traps because the ions are confined in a narrow volume. Lines, therefore, are not Doppler shifted.

The lines generated in an EBIT device may be broadened by Doppler broadening as a result of their thermal motion. They may also be broadened by the response function of the instruments used in their observation. In order to ascertain the thermal motion of the ions, it is necessary to deploy spectrometers with very high resolving powers that do not obscure the x-ray line shape. This is especially the case when the ion temperature is low. Such instrumentation was recently implemented on our electron beam ion trap facilities [18]. Resolving powers exceeding $\lambda/\Delta\lambda = 60,000$ were achieved, enabling the studies presented in this progress report.

This paper is organized as follows. We first present a brief description of how ions are produced and trapped in an EBIT device and describe the spectroscopic instrumentation employed in our measurements. We present measurements of the temperature of the trapped ions inferred from the Doppler-broadened line profiles and discuss our attempts to systematically lower the temperature without degrading the signal to noise of the spectral measurements. We then apply our techniques to the $(2p_{3/2}^5 3d_{5/2})_{J=1} \rightarrow (2p^6)_{J=0}$ transition in neonlike Cs^{45+} and record the Lorentzian shape of the line. From the time-energy relations of the Uncertainty Principle, we determine a 1.65-fs radiative lifetime of the excited level. In the conclusion we briefly discuss possible applications of the spectroscopy of cold ions in atomic and nuclear physics and give specific examples of future measurements.

EBIT OPERATION

The EBIT device employs a monoenergetic 60- μm -diameter electron beam to produce, trap, and excite a particular charge state of interest, as described in detail by Levine *et al.* [19,20]. The interaction between the ions and electrons takes place within the 2-cm-long cylindrical confinement region illustrated in Fig. 1. Confinement of the ions in the axial direction is accomplished by biasing the three drift tubes. In standard operation, an axial trapping potential $V_{ax} = 100 \text{ V}$ is applied. Confinement in the radial direction is accomplished by the space charge potential V_b of the electron beam, which depends on the beam current I and the beam energy E [19]:

$$V_b \approx 0.5(1 - f)I/\sqrt{E}. \quad (1)$$

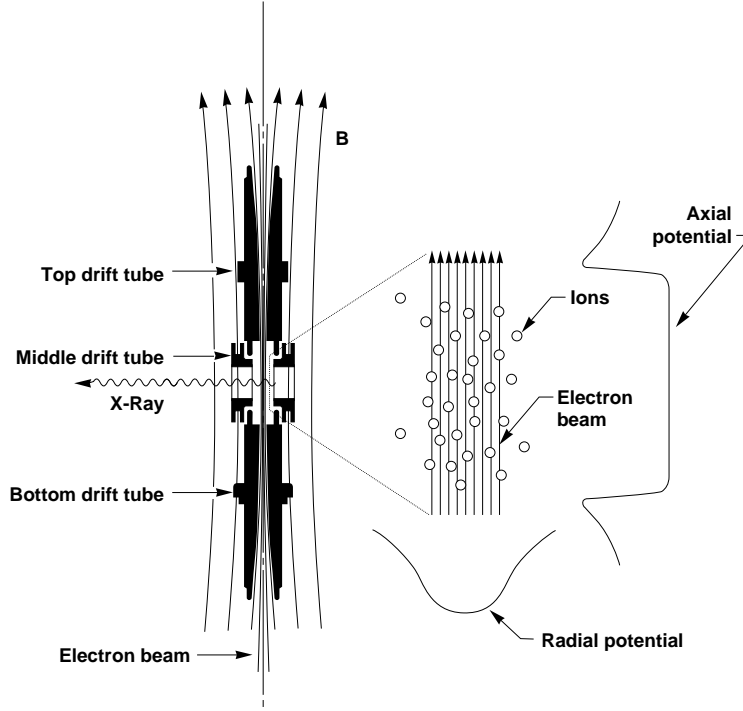


FIGURE 1. Schematic of the trapping geometry of the electron beam ion trap. The ions are trapped axially in the potential applied to the top and bottom drift tubes and radially in the space charge potential of the electron beam. The middle drift tube is slotted to allow a direct view of the trapping region and for recording emitted x rays.

Here, f is the fraction of the beam space charge neutralized by the presence of the ions. In standard operation, the radial potential at the beam edge relative to the beam center is about 10–20 V.

Elastic collisions with the electron beam heats the ions at a rate of several keV/s [19]. The energy gained from this interaction is shared among all ions, as the ion-ion collision frequency is much faster than that of ion-electron collisions [21]. The ions are heated until their kinetic energy is larger than the potential well and they are able to leave the trap. Because low-charge ions experience a potential well that is shallower than the well experienced by ions with higher charge, low-charge ions will leave the trap at a temperature significantly below that necessary for highly charged ions to leave. Loss of highly charged ions can, therefore, be prevented or greatly reduced by providing a constant source of low-charge ions, such as N^{7+} or Ne^{10+} , which carry with them the heat deposited by the electron beam [19,22,23].

The mechanisms of production and trapping suggests the ability to produce highly charged ions with “arbitrarily” low temperature. The temperature of the highly charged ions is limited by the temperature needed for low-charge ions to leave the trap. By reducing the potential well of the trap, this temperature is reduced, and we expect a drop in the overall ion temperature. The

measurements described below confirm our expectation.

SPECTROSCOPIC INSTRUMENTATION

Our measurements concentrated on the ions Ti^{20+} and Cs^{45+} . The two ion species emit K-shell or L-shell x-ray lines, respectively, in the wavelength range 2.60–2.64 Å. The ion temperature T_i is determined from the Doppler broadening of the emitted line radiation $\Delta\lambda$ using the relation

$$T_i = \frac{m_i c^2}{8 \ln 2} \left[\frac{\Delta\lambda}{\lambda} \right]^2, \quad (2)$$

where m_i is the ion mass, c is the speed of light, and λ is the wavelength of the measured transition.

For such measurements to succeed it is necessary to employ spectrometers with very high resolving power. In our measurements, we employed a high-resolution crystal spectrometer based on the geometry proposed by von Hámos [24]. The spectrometer utilized a cylindrically bent analyzing crystal oriented such that the axis of the cylinder lies in the plane of dispersion. The instrument functions like a flat-crystal spectrometer in the plane of dispersion and provides focusing for rays perpendicular to the plane of dispersion. A schematic of the focusing properties of the von Hámos geometry is shown in Fig. 2. The von Hámos geometry is well suited for measurements on an EBIT, because EBIT represents a slit-like line source whose dimensions are determined by the 60- μm -diameter electron beam and the 2-cm-long trap length.

As illustrated in Fig. 2, x rays with different wavelengths λ are focused at different positions along the axis of curvature of the crystal. Aberrations are

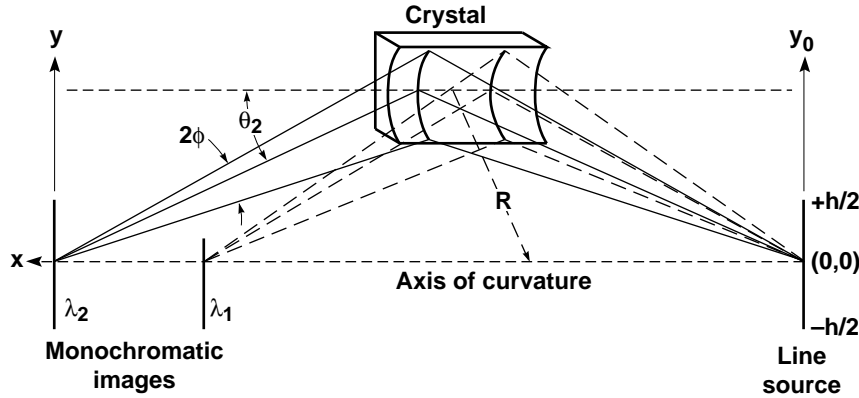


FIGURE 2. Focusing geometry of the EBIT von Hámos-type high-resolution crystal spectrometer. A cylindrically bent crystal generates monochromatic images of the EBIT source at different location along its axis of curvature. The images are recorded with a position sensitive proportional counter.

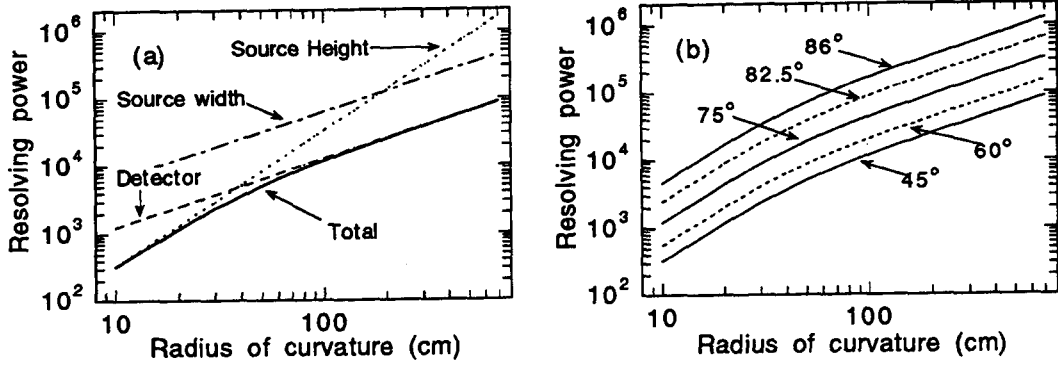


FIGURE 3. Estimated resolving power achievable with a crystal of different radii of curvature. Limitations from a 300- μm spatial resolution of the detector, a 1.2-cm source height, and a 60- μm source width are listed separately in (a). Here, the assumed Bragg angle is 45° . The variation of the resolving power for different Bragg angles is shown in (b).

introduced by the finite height h of the source, the finite diameter of the EBIT source Δs , and the finite spatial resolution of the detector Δx . Using a crystal with a radius of curvature R and an opening angle ϕ less than the Bragg angle θ , the limitation in the resolving power caused by the source height is given by

$$\lambda/\Delta\lambda \approx 4R^2/h^2. \quad (3)$$

The limitation caused by the source diameter is

$$\lambda/\Delta\lambda = 2D \tan \theta / \Delta x. \quad (4)$$

That caused by the finite detector resolution is

$$\lambda/\Delta\lambda = 2D \tan \theta / \Delta s. \quad (5)$$

Here, $D = R/\sin \theta$ is the distance between crystal and detector as well as between crystal and source. The quadratic sum of these aberrations is shown in Fig. 3(a) as a function of the radius of curvature of the crystal. Here, we took $h = 1.2$ cm, $\Delta x = 60$ μm , and $\Delta s = 300$ μm , which were typical values for our setup. The resolving power also varies with $\tan \theta$, as illustrated in Fig. 3(b).

In order to obtain the highest resolving power, we employed a crystal with a large radius of curvature and operated at a large Bragg angle. The layout of our very high-resolution spectrometer on the EBIT device is shown in Fig. 4. Our instrument employs a large, $120 \times 50 \times 0.25$ mm³ quartz($20\bar{2}3$) crystal, which has a lattice spacing $2d = 2.750$ Å. The crystal was bent to a radius of curvature $R = 240$ cm. The nominal resolving power attainable with this crystal was $\lambda/\Delta\lambda = 22,000$ at a Bragg angle $\theta = 45^\circ$. However, the Bragg angle to observe the Ti^{20+} and Cs^{45+} lines was about $\theta = 72^\circ$. Because of the

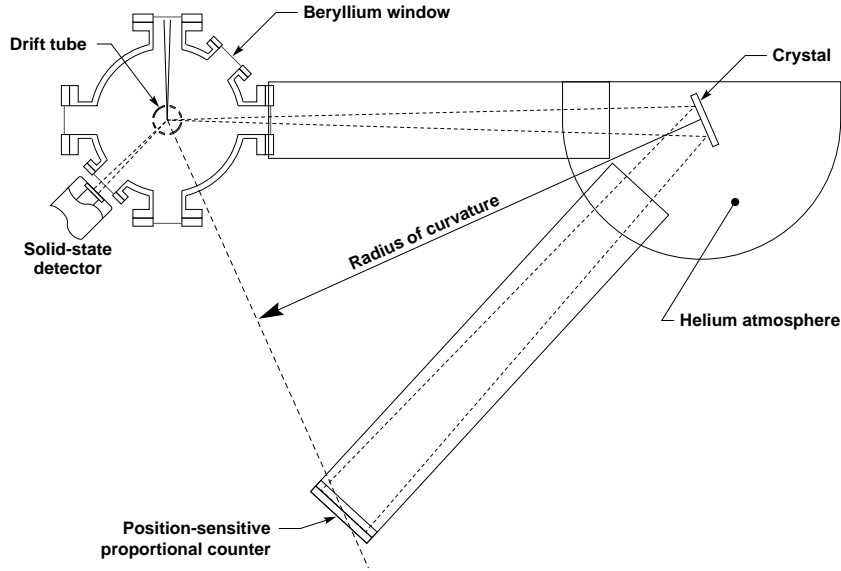


FIGURE 4. Layout of the high-resolution crystal spectrometer on EBIT. The electron beam is out of the page. The spectrometer operates in a helium atmosphere to reduce x-ray absorption by air. The vacuum interface is provided by a 125- μm beryllium window.

$\tan \theta$ dependence the nominal resolving power thus was much higher, i.e., it was increased to $\lambda/\Delta\lambda \geq 66,000$. This value may be reduced by the intrinsic resolving power of crystal. Quartz(20 $\overline{2}$ 3), however, has an intrinsic resolving power of about 200,000 [25]. This is in excess of the nominal resolving power of the spectrometer and does not significantly reduce our estimate.

ION TEMPERATURE MEASUREMENTS

Spectra of the heliumlike Ti^{20+} intercombination lines $1s2p\ ^3P_1 \rightarrow 1s^2\ ^1S_0$, labeled y , and $1s2p\ ^3P_2 \rightarrow 1s^2\ ^1S_0$, labeled x are shown in Fig. 5. These spectra were obtained for two different operating conditions. The first was obtained with a beam current $I = 131\text{ mA}$ and an axial well potential $V_{ax} = 200\text{ V}$. The second was obtained with a beam current $I = 51\text{ mA}$ and an axial well potential $V_{ax} = 0\text{ V}$. The beam energy in both cases was about 5 keV. This value equaled the energy to excite some of the KMM resonances. These resonances enhanced the line emission of lines x and y by nearly a factor of two over the emission produced by direct electron-impact excitation alone [26]. The electron-ion interaction energy was slightly different for the two spectra because of the change in the space charge of the electron beam as the beam current was changed. As a result, a somewhat different set of KMM resonances was excited, and the relative intensities of lines x and y varied between two spectra.

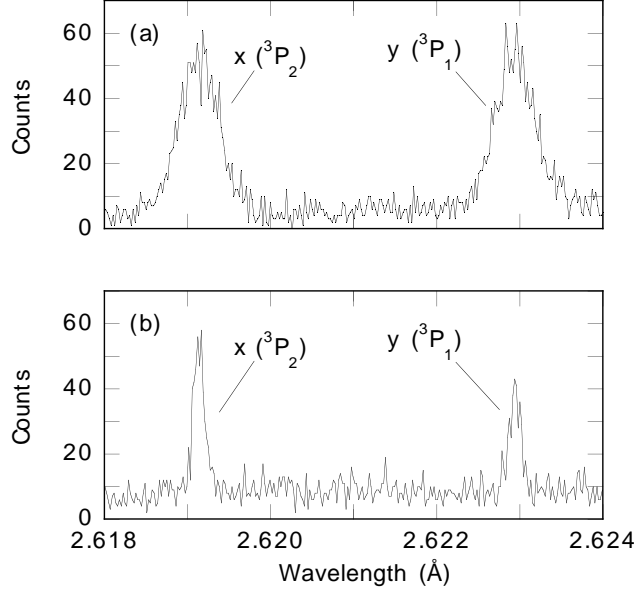


FIGURE 5. Spectra of the heliumlike Ti^{20+} intercombination lines $1s2p\ ^3P_2 \rightarrow 1s^2\ ^1S_0$ and $1s2p\ ^3P_1 \rightarrow 1s^2\ ^1S_0$, labeled x and y , respectively, obtained for two different EBIT operating conditions. The ion temperatures inferred from the line widths are 368 ± 22 and 31.2 ± 4.2 eV.

The measured line widths in Fig. 5(a) are $0.56\ \text{m}\text{\AA}$. These correspond to a temperature of 368 ± 22 eV. The line widths in (b) are $0.16\ \text{m}\text{\AA}$ and correspond to an ion temperature of 31.2 ± 4.2 eV. By contrast, the resolving power of the spectrometer corresponds to an effective ion temperature of 1.8 eV and does not contribute to the observed line widths.

The reduction in the temperature evident in Fig. 5 was achieved by reducing the axial potential and the beam current, i.e., the radial potential. The effect of each parameter separately on the ion temperature is seen in Fig. 6. In Fig. 6 (a) we plot the inferred ion temperature as a function of the applied axial potential V_{ax} . The current was kept constant at 130 mA. Reducing V_{ax} from 200 V to 0 V reduced the ion temperature from about 300 eV to slightly below 100 eV. Fixing the axial potential at $V_{ax} = 0$ V, the temperature can be lowered further by reducing the beam current. A reduction from 130 mA to 50 mA lowered T_i from about 100 to about 30 eV. In fact, we observed a temperature as low as 15.8 ± 4.4 eV under these conditions.

In Fig. 6 we also plot the dependence of the temperature of Cs^{45+} ions on the applied potential and electron beam current. The temperature was inferred from the observed Gaussian line width of the $(2p_{1/2}^5 3s_{1/2})_{J=1} \rightarrow (2p^6)_{J=0}$ transition. This line is located at $2.6079\ \text{\AA}$, and thus falls into the same wavelength region as the titanium lines. A description of the spectrum is given in the next Section. The Cs^{45+} ions were excited by a 7.5-keV electron beam, i.e., at an

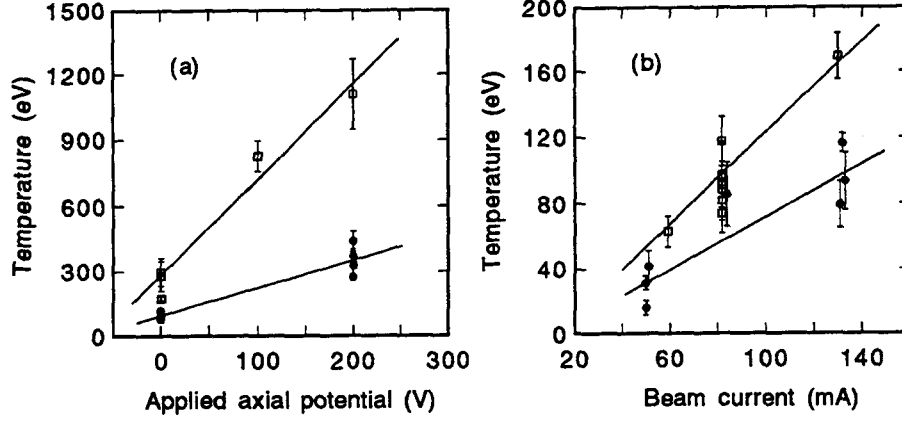


FIGURE 6. Dependence of the inferred ion temperature on (a) the applied axial potential and (b) electron beam current. Solid circles represent data from heliumlike Ti^{20+} , open squares from neonlike Cs^{45+} . The solid lines represent least-squares fits to the data and are shown as a guide to the eye only.

energy about 50% larger than that for the Ti^{20+} measurements.

The Cs^{45+} data show a similar dependence on the trap parameters as the titanium data. Lowering the potential well from 200 to 0 V reduced the temperature of the ion from well about 1200 eV to 300 eV. A further reduction was achieved by lowering the electron beam current. Choosing a beam current of 59 mA and an axial trap of 0 V, we measured an ion temperature of 59.4 ± 9.9 eV.

The temperature of the Cs^{45+} ions is systematically higher than that of the Ti^{20+} ions. In fact, a difference of about a factor of two to three is found. However, because the charge of the Cs^{45+} ions is higher than that of the titanium ions we expect them to be more deeply bound in the trap. Dividing the measured temperature by the charge of the ion provides a measure of the effective trapping potential. This value is about the same for both ion species for similar trapping parameters. Values less than 1 V/q are found for the shallowest trap conditions.

The low temperatures measured for shallow trap conditions contrast starkly with the temperatures measured in deep traps. The highest temperature we measured for Ti^{20+} was 439 ± 47 eV. The parameters for this measurement were $I = 135$ mA, $V_{ax} = 200$ V, and $E_{beam} = 6.5$ keV. The highest temperature for Cs^{45+} was 1145 ± 72 eV at a beam current of 145 mA, a beam energy of 7.5 keV, and an applied potential of 300 V.

OBSERVATION OF LORENTZIAN LINE WIDTHS

By the Heisenberg time-energy relations [27], electric dipole x-ray transitions in highly charged ions exhibit a large energy uncertainty. Based on the Dirac equation, Weisskopf and Wigner showed that this uncertainty results in a lifetime-limited, Lorentzian-shaped “natural” line width [28]. For an excited state decaying to the ground state, the line width ΔE is given by

$$\Delta E = \hbar / \Delta t, \quad (6)$$

where Δt is the excited-state lifetime.

A line width $\Delta E = 0.658$ eV results for a lifetime of $\Delta t = 1$ fs. Such a width would be relatively easy to measure in a visible or UV transition, where ΔE represents a large fraction of the overall transition energy. We note, though, that the transition rates for such transitions are typically no more than 10^{13} s⁻¹ reducing the natural line width accordingly. By contrast, it is much more difficult to measure a Lorentzian width in the x-ray regime, where it represents a rather small fraction of the x-ray energy.

In the following we concentrate on measuring the natural line width of the $(2p_{3/2}^5 3d_{5/2})_{J=1} \rightarrow (2p^6)_{J=0}$ x-ray transition in neonlike Cs⁴⁵⁺. This line is situated within 7.2 mÅ from the $(2p_{1/2}^5 3s_{1/2})_{J=1} \rightarrow (2p^6)_{J=0}$ transition, thus allowing observation of the two lines in a single spectrum with the same spectrometer arrangement described above. The radiative lifetime of its upper level is predicted in single-configuration calculations to be 1.39 fs, which corresponds to natural line width of 0.47 eV.

The natural line width of the $(2p_{3/2}^5 3d_{5/2})_{J=1} \rightarrow (2p^6)_{J=0}$ transition is easily masked by other broadening effects. To produce neonlike Cs⁴⁵⁺ ions in the Princeton Large Tokamak required an electron temperature of about 5 keV [29]. Assuming an ion temperature of just half the electron temperature, the thermal broadening is more than three times the Lorentzian width of the $2p$ - $3d$ transition, and the natural line width is obscured.

The natural line broadening of the $2p$ - $3d$ transition should become obvious provided the ion temperature is less than about 200 eV, i.e., for temperatures where the Doppler-broadened line width is less than the natural width. By contrast, the predicted natural width of the $2p$ - $3s$ transition is predicted to be an order of magnitude smaller than the instrumental broadening and cannot be observed. In our measurements, the $2p$ - $3s$ line serves instead as an indicator of the temperature of the Cs⁴⁵⁺ ions. The observed width was typically $\Delta E \geq 0.25$ eV with a Gaussian lineshape indicative of thermal Doppler broadening, from which the ion temperature T_i was determined.

Three spectra of the $2p$ - $3d$ and $2p$ - $3s$ transitions obtained under different operating conditions are shown in Fig. 7. The reduction in the width of both lines as the temperature is lowered is clearly seen. Unlike for the $2p$ - $3s$ line, the reduction in width nearly ceases for the $2p$ - $3d$ line at the lowest temperatures,

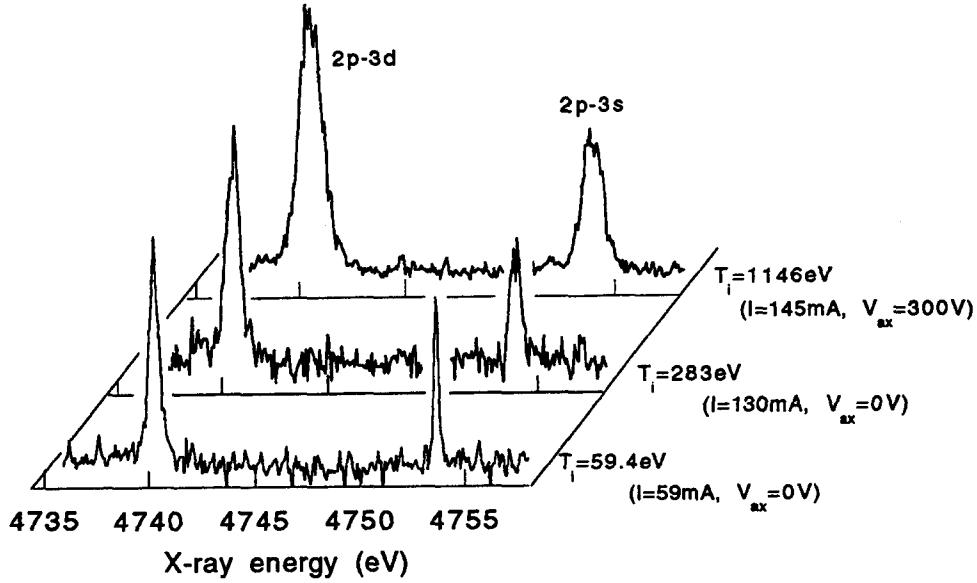


FIGURE 7. Spectra showing the two x-ray transitions from upper levels $(2p_{3/2}^5 3d_{5/2})_{J=1}$ and $(2p_{1/2}^5 3s_{1/2})_{J=1}$ to the $(2p^6)_{J=0}$ closed-shell neonlike ground state in Cs^{45+} . The ion temperature T_i inferred from the width of the $2p-3s$ line drops from 1146 eV to 59.9 eV as the electron beam current I and axial trapping potential V_{ax} are reduced to the values indicated.

and the Lorentzian line shape becomes evident. A detailed view of the line shape of the $2p-3d$ transition recorded at an ion temperature of 110 eV is given in Fig. 8. Fitting the line with a Lorentzian trial function provides an excellent fit. The goodness of the fit is indicated by the reduced residuals shown in Fig. 8(a), which are defined as the difference between data and fit normalized to the square root of the fit value at each point. By contrast, fitting the line with a Gaussian trial function provides a poor fit, as illustrated in Fig. 8(b).

Residual contributions of thermal broadening on the line shape are accounted for by fitting the $2p-3d$ line with a Voigt profile [30], which represents a Lorentzian convolved with a Gaussian profile. For this, the temperature parameter for the Gaussian profile is taken from the width of the $2p-3s$ line. A value of 0.398 eV averaged over all observations was obtained for the natural width of the $2p-3d$ line. The statistical uncertainty is ± 0.012 eV. A systematic uncertainty is introduced by the possibility that natural broadening may also affect the width of the $2p-3s$ line. This would result in an inferred temperature that is too high. Because of the close vicinity of the upper level of each line, configuration interaction might decrease the lifetime of the $(2p_{3/2}^5 3s_{1/2})_{J=1}$ level while decreasing that of the $(2p_{3/2}^5 3d_{5/2})_{J=1}$ level. No lifetime-limited line broadening of the $2p-3s$ line was detected within the resolution of our measurements. However, the minimum amount detectable with our technique

introduces a systematic error of -0.049 eV, which combines with the statistical uncertainty and yields a natural line width of $0.398^{+0.012}_{-0.050}$ eV for the $2p\text{-}3d$ line. From this we infer a radiative lifetime of the excited level of 1.65 fs with an uncertainty of $+0.24$ fs and -0.05 fs.

The measured value differs from the 1.39 fs predicted by single-configuration calculations. Allowing for configuration interaction by including all 36 excited levels with a vacancy in the $n = 2$ shell and an excited electron in the $n = 3$ shell in a multi-configuration Dirac-Fock calculation in the extended average level (EAL) model as described by Grant *et al.* [31], we get 1.98 fs. This value also differs from the observed value, albeit in the opposite direction than the single-configuration result. This disagreement with theory as well as between theoretical approaches shows that measurements are needed even for very fast electric dipole transitions in order to guide atomic calculations, especially when configuration interactions play a dominating role.

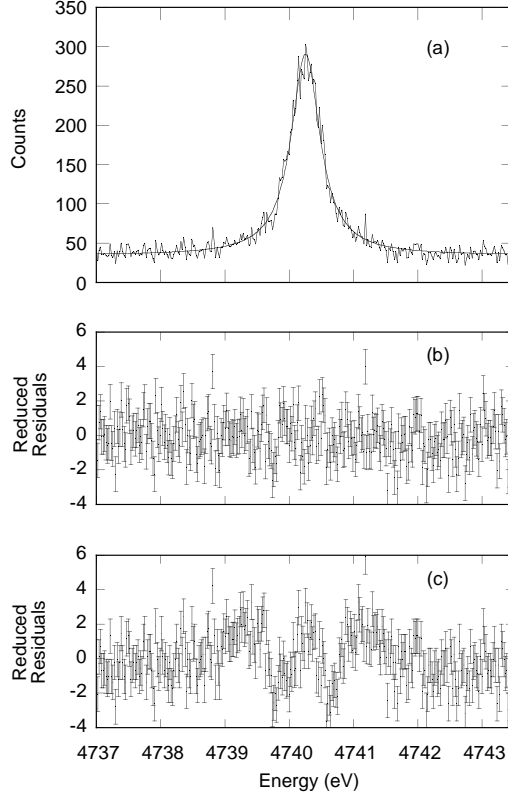


FIGURE 8. Observed lineshape of the $2p\text{-}3d$ transition at an ion temperature of 110 eV. The result of a least-squares fit of a Lorentzian trial function is superimposed for comparison. The reduced residuals of the fit are shown in (b). The reduced residuals of a least-squares fit of a Gaussian trial function are shown in (c).

DISCUSSION

Our measurements have demonstrated that the temperature of the ions in an electron beam ion trap can be reduced to values below $1 \text{ V}/q$ despite continuous interactions with a multi-keV electron beam. A decoupling of the energy of the ions from that of the electrons employed for production and excitation by more than two orders of magnitude was achieved by reducing the potential well of the trap and by allowing the hottest ions to leave. Although the total number of ions in the trap dropped as the potential well was reduced, enough ions remained to prevent a significant degradation of the signal-to-noise ratio, as seen in Figs. 5 and 7. In fact, further decoupling appears possible. Because fewer photons are needed to map out a narrower line, the peak line intensity, and thus the signal-to-noise ratio, can be expected to remain nearly constant relative to the background level as the potential well and the ion energy are reduced further. Such a decoupling is crucial for precision measurements, since in the absence of x-ray or gamma-ray lasers, probing by energetic electrons is the method of necessity for studying the structure of highly charged ions.

Cooling, i.e., the reduction in the translational motion, has been applied effectively to atoms and singly charged ions to increase the precision and range of fundamental atomic and nuclear physics measurements [1]. In our progress report we showed that a controlled reduction in the translational energy is now possible for highly charged ions as well.

The production of low-temperature highly charged ions opens up a multitude of high precision studies. We have already shown that it is possible to perform measurements of the radiative lifetimes in the femtosecond regime. In this regime, no such measurements have been possible before. The fastest radiative lifetimes measured by other techniques are three orders of magnitude lower, in the ten-picosecond range [6,7]. Theoretical calculations of femtosecond radiative lifetimes, thus, have never before been validated by a measurement.

The production of low-temperature highly charged ions also allows measurements of energy levels with unprecedented accuracy. In the present measurements, relative x-ray line widths as low as $\Delta\lambda/\lambda = 5 \times 10^{-5}$ have been achieved. Because the location of a line can typically be determined to within better than a tenth of the value of its width, such small line widths, in principle, enable determinations of x-ray transition energies with a precision of one part per million with relative ease. Very precise tests of relativistic energy calculations and of QED contributions are thus possible.

Precise energy level determinations also play an important role in x-ray laser research. Here, coincidences between two x-ray lines could be used for resonant photopumping of lasing transitions. Examples are given in Refs. [32–34]. A precise experimental determination of the degree of overlap between two lines is essential for validating the feasibility of a proposed photopumping scheme.

The production of low-temperature highly charged ions also enables possible

observations of x-ray lines split by the hyperfine interaction. Two obvious candidates are the $2s_{1/2}-2p_{1/2}$ and the $2s_{1/2}-2p_{3/2}$ transitions in lithiumlike Bi^{80+} . These transitions are split by about 0.8 eV [35]. This splitting requires a minimum resolving power of $\lambda/\Delta\lambda = 3000$ for the $2s_{1/2}-2p_{3/2}$ transition. This can only be achieved, if the ion temperature is decoupled from the estimated minimum electron energy of 30–50 keV needed for the production of such a highly charged ion.

As a final example of the possibilities created by the production of low-temperature highly charged ions we mention measurements of the isotopic variation of nuclear charge radii. The feasibility of such measurements using highly charged ions has been demonstrated just recently [36] in a measurement of ^{233}U and ^{238}U . The uncertainties associated with this measurement were comparable to the uncertainties associated with the more standard methods of determining variations in nuclear charge radii. Using low-temperature ions for such a measurement could reduce the uncertainty by nearly an order of magnitude and thus make this method the method of choice for the measurement of such fundamental nuclear parameters.

ACKNOWLEDGMENTS

This work was performed at the Lawrence Livermore National Laboratory under the auspices of the Department of Energy under Contract No. W-7405-Eng-48. Support from the Office of Basic Energy Sciences is gratefully acknowledged.

REFERENCES

1. *Atomic Physics 14*, AIP Conference Proceedings No. 323, ed. by D. J. Wineland, C. E. Wieman, and S. J. Smith (AIP, New York, 1995), p. 193-275.
2. W. M. Itano, J. C. Bergquist, J. J. Bollinger, and D. L. Wineland, *Phys. Scripta* **T59**, 106 (1995).
3. P. Beiersdorfer, V. Decaux, and K. Widmann, *Nucl. Instrum. Methods* **B98**, 566 (1995).
4. P. Beiersdorfer, A. L. Osterheld, V. Decaux, and K. Widmann, (submitted to *Phys. Rev. Lett.*) (1996).
5. S. Diehl *et al.*, *Phys. Rev. Lett.* **76**, 3915 (1996).
6. L. Engström and P. Bengtsson, *Phys. Scripta* **43**, 480 (1991).
7. S. Cheng *et al.*, *Phys. Rev. A* **50**, 2197 (1994).
8. B. A. Hammel *et al.*, *Phys. Rev. Lett.* **70**, 1263 (1993).
9. C. J. Keane, B. A. Hammel, A. L. Osterheld, and D. R. Kania, *Phys. Rev. Lett.* **72**, 3029 (1994).
10. M. Bitter *et al.*, *Phys. Rev. Lett.* **42**, 304 (1979).

11. J. L. Culhane *et al.*, *Astrophys. J.* **244**, L141 (1981).
12. T. S. Perry *et al.*, *Phys. Rev. Lett.* **67**, 3784 (1991).
13. M. J. Seaton, Yu Yan, D. Mihalas, and A. K. Pradhan, *Mon. Not. R. Astron. Soc.* **266**, 805 (1994).
14. P. Beiersdorfer *et al.*, in *UV and X-Ray Spectroscopy of Astrophysical and Laboratory Plasmas*, ed. by E. Silver and S. Kahn (Cambridge University Press, Cambridge, 1993), p. 59.
15. F. Bely-Dubau, A. H. Gabriel, and S. Volonté, *Mon. Not. R. Astron. Soc.* **189**, 801 (1979).
16. M. Bitter *et al.*, *Phys. Rev. Lett.* **47**, 921 (1981).
17. A. A. Hauer, N. D. Delameter, and Z. M. Koenig, *Laser and Particle Beams* **9**, 3 (1992).
18. P. Beiersdorfer, V. Decaux, S. Elliott, K. Widmann, and K. Wong, *Rev. Sci. Instrum.* **66**, 303 (1995).
19. M. A. Levine, R. E. Marrs, J. R. Henderson, D. A. Knapp, and M. B. Schneider, *Phys. Scripta* **T22**, 157 (1988).
20. M. A. Levine *et al.*, *Nucl. Instrum. Methods* **B43**, 431 (1989).
21. L. Spitzer, *The Physics of Ionized Gases* (J. Wiley & Sons, New York, 1962).
22. M. B. Schneider, M. A. Levine, C. L. Bennett, J. R. Henderson, D. A. Knapp, and R. E. Marrs, in *International Symposium on Electron Beam Ion Sources and their Applications - Upton, NY 1988*, AIP Conference Proceedings No. 188, edited by A. Hershcovitch (AIP, New York, 1989), p. 158.
23. B. M. Penetrante, J. N. Bardsley, M. A. Levine, D. A. Knapp, and R. Marrs, *Phys. Rev. A* **43**, 4873 (1991).
24. L. v. Hámos, *Ann. der Physik* **17**, 716 (1933).
25. A. Burek, *Space Sci. Instrum.* **2**, 53 (1976).
26. S. Chantrenne, P. Beiersdorfer, R. Cauble, and M. B. Schneider, *Phys. Rev. Lett.* **69**, 265 (1992).
27. W. Heisenberg, *Z. Phys.* **43**, 172 (1927).
28. V. Weisskopf and E. Wigner, *Z. Phys.* **63**, 54 (1930).
29. P. Beiersdorfer *et al.*, *Phys. Rev. A* **37**, 4153 (1988).
30. A. Unsöld, *Physik der Sternatmosphären*, 2nd ed. (Springer-Verlag, Berlin, 1955).
31. I. P. Grant, B. J. McKenzie, P. H. Norrington, D. F. Mayers, and N. C. Pyper, *Comput. Phys. Commun.* **21**, 207 (1980).
32. R. C. Elton, *Phys. Rev. A* **38**, 5426 (1988).
33. J. Nilsen, *Phys. Rev. Lett.* **66**, 305 (1991).
34. P. Beiersdorfer *et al.*, *Phys. Rev. A* **46**, R25 (1992).
35. V. M. Shabaev, M. B. Shabaev, and I. I. Tupitsyn, *Phys. Rev. A* **52**, 3686 (1995).
36. S. R. Elliott, P. Beiersdorfer, and M. H. Chen, *Phys. Rev. Lett.* **76**, 1031 (1996).